Journal of South American Earth Sciences 63 (2015) 36–47

Contents lists available at ScienceDirect

Journal of South American Earth Sciences

journal homepage: www.elsevier.com/locate/jsames

Triggered seismicity in the Andean arc region via static stress variation by the $M_W = 8.8$, February 27, 2010, Maule earthquake

Silvana Spagnotto [a, *], Enrique Triep [b], Laura Giambiagi [c], Marianela Lupari [b]

[a] Departamento de Física, Universidad Nacional de San Luis, Ejército de los Andes 950, 5700, San Luis, Argentina
[b] Instituto Geofísico-Sismológico Ing. F. S. Volponi, Universidad Nacional de San Juan, Ruta 12, Km 17, CP 5407, San Juan, Argentina
[c] IANIGLIA-CCT, Mendoza-CONICET, Argentina

ARTICLE INFO

Article history:
Received 5 August 2014
Received in revised form
12 June 2015
Accepted 29 June 2015
Available online 7 July 2015

Keywords:
Triggered seismicity
Static stress variation
Andean arc region

ABSTRACT

We localized crustal earthquakes in the Andean arc, between 35°S and 36°S, from December 2009 to May 2010. This research shows a seismicity increase, in a narrow longitudinal area, of more than nine times after the great M_w 8.8 Maule earthquake.

The localized seismicity defines an area of ~80 km long and ~18 km wide and NNW to NNE trend. The M_d magnitudes varied from 0.7 to 3.1 except for two earthquakes with M_w of 3.9 and 4.5, located in the northern end of the area. The focal mechanisms for these two last events were normal/strike-slip and strike-slip respectively.

During 2011, a network of 13 temporary stations was installed in the trasarc region in Malargüe, Argentina. Sixty earthquakes were localized in the study region during an 8 month period.

We explored how changes in Coulomb conditions associated with the mega-thrust earthquake triggered subsequent upper-plate events in the arc region. We assumed the major proposed structures as receiver faults and used previously published earthquake source parameters and slip distribution for the Maule quake. The largest contribution to static stress change, up to 5 bars, derives from unclamping resulting consistent with co-seismic dilatational deformation inferred from GPS observations in the region and subsidence in nearby volcanoes caused by magma migration.

Three different Quaternary tectonic settings—extensional, strike-slip and compressional-have been proposed for the arc region at these latitudes. We found that the unclamping produced by the Maule quake could temporarily change the local regime to normal/strike-slip, or at least it would favor the activation of Quaternary NNE to N-trending dextral strike-slip faults with dextral transtensional movement.

1. Introduction

One of the most significant questions in seismology involves the change in short-term upper-plate seismicity after a major inter-plate earthquake. Multiple lines of evidence indicate that the brittle crust is critically stressed and in a state of incipient failure (Bak and Tang, 1989; Cowie et al., 1993; Zoback and Zoback, 2002). Therefore, small stress changes produced by a near or distant earthquake could trigger ruptures in the continental crust, as shown by King et al. (1994) and Freed (2005).

This is reinforced by several studies showing activation of crustal seismicity by static stress changes in the upper-plate of a subduction region caused by a great earthquake in the mega-thrust fault (King et al., 1994; Ryder et al., 2012; Rietbrock et al., 2012 and Aron et al., 2013). Taylor et al. (1998) particularly deal with upper-plate seismicity in Irian Jaya, Indonesia, preceding and immediately following the February 17, 1996, $M_w = 8.2$ earthquake. The focal mechanisms, normal in one zone and strike-slip in the other one, are explained by subduction obliquity and relative position of the greater asperity.

Since the beginning of instrumental seismology, the M_w 8.8 Maule earthquake on 27 February 2010 is among the ten biggest ones. Several studies have pointed out that this earthquake increased the seismicity in the region. Lange et al. (2012) recorded 20205 aftershocks with Mw magnitudes between 1 and 5.5. Most of their hypocenters were located in the inter-plate region. However, several earthquakes in the upper-plate have presented normal faulting mechanisms. Farías et al. (2011), Ryder et al. (2012), Rietbrock et al. (2012) and Aron et al. (2013) showed activation of

* Corresponding author.
E-mail address: pampa113@gmail.com (S. Spagnotto).

http://dx.doi.org/10.1016/j.jsames.2015.06.009
0895-9811/

crustal earthquakes near the continental border with normal focal mechanisms as a consequence of the earthquake. Pritchard et al. (2013) show the subsidence of five calderas in the Andean Southern Volcanic Zone following the Maule earthquake, and they associate it to the coseismic release of fluids at hydrothermal systems.

Freed (2005), and Gomberg et al. (2003) suggests that if dynamic stress changes are strong enough to trigger earthquakes at distances out of several hundred kilometers, there is no reason why such stresses should not trigger aftershocks or earthquakes at distances comparable to a single fault length or less. At nearer distances, it is very difficult to differentiate dynamic stress changes from the static ones. In our case, the rupture directivity, where dynamic change is more important, was northwards (USGS, http://earthquake.usgs.gov/earthquakes/eventpage/usp000h7rf#scientific_finitefault); meanwhile the earthquakes were in the east. On the other hand, Hill et al. (1993) and Anderson et al. (1994), suggest that the dynamic stress decay occurs in approximately a day while this seismicity lasted for three months. Even so, Belardinelli et al. (2003) found that dynamic stress always promotes failure, and never inhibits the seismicity.

Jay et al. (2012) associate the increased seismicity at the Uturuncu volcano in southern Bolivia, with the passage of surface waves, as well as Peng et al. (2010) relate them with the microearthquakes near the Coso Geothermal Field, California.

Scott et al. (2014) analyzed the role of the Maule earthquake in triggering shallow earthquakes in Argentina and Chile. They show ground deformation associated with the Mw 6.2 Salta, Mw 5.8 Catamarca, and additional earthquakes using Interferometric Synthetic Aperture Radar (InSAR). The Salta and Catamarca earthquakes are broadly consistent with regional late Cenozoic fault kinematics. They infer that dynamic stresses due to the passage of seismic waves would advance the seismic cycle, but they do not estimate values for these regions.

This study reports upper-plate seismicity activation in the Andean arc region, between 35°S and 36°S. It explores Coulomb static stress changes caused by the Maule earthquake and proposes that a small stress change in the arc region produced during this quake was responsible for a seismically active NNE to N striking dextral strike-slip fault.

2. Coulomb criterion

The tendency of rock to fail in a brittle manner is thought to be a function of both shear and normal stresses on pre-existing planes, commonly formulated as the Coulomb failure criterion. Earthquakes take place when the shear stresses are larger than the normal (or clamping) stresses that, in combination with friction, inhibit a locked fault from slipping (Freed, 2005). Slippage on a fault, such as the Maule earthquake mega-thrust fault, changes the stress field around it, and may activate seismicity.

Failure occurs when the Coulomb stress change is higher than the specific value $\Delta\sigma_f = \Delta\tau_s + \mu'\Delta\sigma_n$, where $\Delta\tau_s$ and $\Delta\sigma_n$ are the shear and normal stress changes on the failure plane respectively, and μ' is the effective coefficient of friction which incorporates the pore pressure effect on $\Delta\sigma_n$ (King et al., 1994; Kilb et al., 2002). In the $\Delta\sigma_f$ expression, $\Delta\tau_s$ must always be chosen positive, and $\Delta\sigma_n$ is positive in the unclamping direction, hence corresponding to the block separation. Even though experimental results at high normal stress indicate that μ' is close to a 0.6 value independently of rock type (Byerlee, 1978) other authors discuss different values of μ' (Parsons et al., 1999; Lin and Stein, 2004). For our Coulomb modeling we use μ' values of 0.4, 0.6 and 0.8 to evaluate the Coulomb stress change in all cases.

The Coulomb criterion has been widely used to show that an earthquake can enhance or suppress subsequent events due to movement along nearby pre-existing faults, depending on their location and orientation. In particular, aftershocks can occur on sites where the stress has increased on or close to the ruptured fault (Stein, 1999; Toda and Stein, 2002). In some cases, stress changes as small as ±0.1 bar are able to induce or inhibit aftershocks (Stein, 1999). In the M_w = 6.9 1995 Kobe, Japan earthquake, a 5 bar stress change has been associated with a 100-fold rate increase of shocks with $M_L \geq 2.6$ (Stein, 1999). For the M_w = 6.9 1989 Loma Prieta, California earthquake, the seismicity rate change in major faults within 100 km from the main fault is associated with calculated shear stress changes (Parsons et al., 1999).

3. Tectonic setting

The seismicity studied in this work is located along the Southern Central Andes volcanic arc, between 35° and 36°S latitude, in the morphostructural unit known as Principal Cordillera. The arc region at these latitudes (Fig. 1) is characterized by a volcanic-arc basement composed of Meso-Cenozoic volcano-sedimentary rocks deformed into the Malargüe fold-and-thrust belt, locally intruded by Mio-Pliocene plutons (Kozlowski et al., 1993; Godoy et al., 1999; Charrier et al., 2002; Folguera et al., 2005a, 2005b; Giambiagi et al., 2008; Tapia et al., 2015; Mescua et al., 2013). The volcanic arc is formed by Pleistocene calderas and volcanic centers (~1.5 a 0.1 Ma, Folguera et al., 2006; Ramos and Kay, 2006) aligned along both NNE and NNW strips.

During the late Triassic to early Jurassic, extension in the Neuquén basin aperture was characterized by the development of several isolated depocenters with master faults striking NW to NNE (Manceda and Figueroa, 1995; Vergani et al., 1995; Giambiagi et al., 2009; Mescua et al., 2013). Triassic-Jurassic depocenters, located north of 35.5°S, were controlled by the NNE trending Río del Cobre master fault (Mescua et al., 2013) while to the south of 35.5°S, is inferred to have been controlled by movement along a NNW trending Río Grande master fault (Manceda and Figueroa, 1995).

During the upper Eocene to lower Miocene, Abanico extensional basin was formed with N to NNE-trending and located immediately to the west of the Neuquén basin (Godoy et al., 1999; Charrier et al., 2002). Its eastern border is inferred to be marked by the high-angle N to NNE-trending La Gloria fault (Parada, 2008), or Infiernillo-Los Cipreces fault (Piquer et al., 2010) (Fig. 1).

During the middle Miocene, a compressive event provoked the inversion of the N to NNE-trending La Gloria pre-existing normal fault (Parada, 2008). During the subsequent deformation, the pre-existing Río del Cobre fault was reactivated (Tapia et al., 2015; Mescua et al., 2013) back-tilting the La Gloria fault up to its subvertical position. In this compressive stage, there is no evidence for the reactivation of the normal Río Grande fault.

In the Pleistocene-Holocene, a series of calderas and volcanic complex are aligned along a NNW strip were developed, from the Azufre-Planchón-Peteroa volcanic complex to its south (Tormey, 2010; Tormey et al., 1989, 1995; Haller and Risso, 2011). This strip has been assigned by Folguera et al. (2005a,b and 2006) to the Las Loicas extensional trough. These authors suggest the existence of a normal fault with NNW strike aligned with the Grande river, whereas, active volcanoes located between 35° and 36°30′S, Peteroa, Descabezado-Quizapu, Cerro Azul and San Pedro-Pellado, are aligned along a NNE strip (Cembrano and Lara, 2009). Several WNW trending lineaments have been identified in the arc region, such as the Atuel (Barrientos et al., 2004; Bechis et al., 2010), Santa Elena (Mescua et al., 2013) and Tinguiririca (Parada, 2008). Some of these lineaments have been suggested to be associated with Mesozoic rift structures (Bechis et al., 2010).

As regards the seismicity in the Southern Central Andes, the largest earthquakes registered at the latitudes analyzed in this paper are: M_w = 6.5, 2004/8/28 and M_w = 6, 2012/6/7, being these the only ones with solutions in CMT catalog. These solutions are strike slip

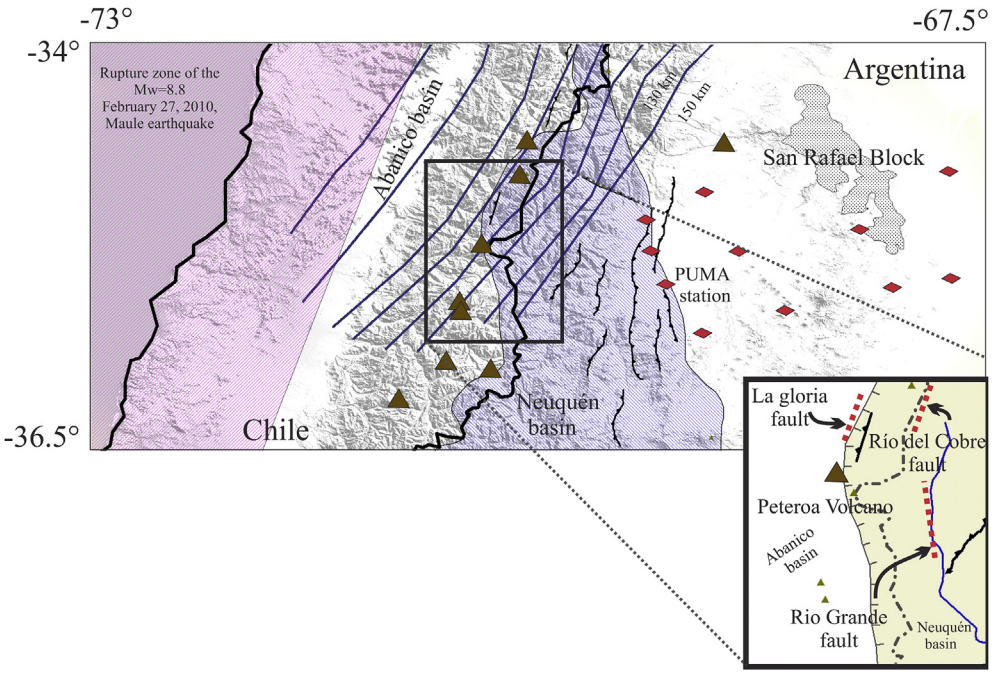

Fig. 1. Main geological features in the study arc region. Part of the rupture zone of the Maule Earthquake is outlined. The shaded area indicates the extension of the Mesozoic of the Neuquén basin. Red Diamonds show location of seismological stations. Blue lines correspond to depth to the subducted Nazca plate from Anderson et al. (2007). (For interpretation of the references to color in this figure legend, the reader is referred to the web version of this article.).

focal mechanism, which would be associated to the subduction obliquity of Nazca plate. Lira Martinez (2011) located post Maule earthquake seismicity, with a local network in the Tinguiririca volcano region and he associated it with the eastern edge of the Abanico extensional basin, but he does not solve focal mechanisms.

4. Data, methodology and seismicity analysis

Since 2009, the data was provided by two temporary digital seismic stations located in the back arc region of Malargüe, Mendoza Province, Argentina (Fig. 1). The stations are COIH (35.11°S, 69.60°W, 1715 m) with an intermediate-band width tri-axial sensor Guralp CMG-EDU, and PUMA (35.50°S, 69.45°W, 1423 m) with three S13 Geotech-Teledyne short-period sensors (vertical and horizontals). During 2011, the network was expanded to 13 new stations (Fig. 1). Three of these stations correspond to Guralp-40T broad-band sensors while the rest are S13 Geotech-Teledyne short-period sensors. Locations and focal mechanisms for two events (Table 1) were obtained with additional data from the Maule Earthquake Aftershock Experiment, and for a third one with the CHARGE experiment.

P and S wave arrival times were picked using SEISAN software (Ottemöller et al., 2012). Earthquake localizations during 2009–2010 were obtained with the PUMA station and in some cases with the COIH station. The time difference between S and P waves (S–P time) were used to calculate hypocentral distance and an average depth of ~12 km for all the earthquakes (Fig. 2). The P waveforms with the three components of the PUMA and COIH stations were correlated to obtain the hypocenter ray azimuth. In order to reduce the localization errors both solution sets were plotted (Appendix A) taking as valid results the intersection between the two of them. The seismicity registered in PUMA and COIH from 1/12/2009 to 31/5/2010, shows an anomalous azimuthal dispersion within the circular sectors with center at the stations. The location errors are large and difficult to evaluate because the magnitude range is $0.7 \leq M_c \leq 3.1$ (Fig. 3a) and the signal to noise ratio is low. Nevertheless, the analysis focuses on the epicenters amassed in a central area with low azimuthal dispersion and errors along the horizontal projection not greater than ±9 km (Fig. 4, and Appendix A).

S–P time histograms (Fig. 2) show concentration between 10 and 14 s, implying a crustal seismicity. The seismicity within the subducted Nazca place, located more than 175 km depth below the PUMA station (Fig. 1), is discarded because the S–P time would be bigger than 16 s.

For earthquakes occurred in 2011–2012 we used HYPOCENTER (Lienert et al., 1986; Lienert and Havskov, 1995) and Join Hypocenter Determination (Douglas, 1967) software (Table 2). The 2011–2012 seismicity errors are indicated with ellipses, and their length is never longer than 30 km (Fig. 4). For every earthquake (2009–2012) we use the velocity model of Spagnotto (2013).

Because the errors are big, we analyzed the possibility of the fault reactivation in the region. In Table 3 these results are shown, considering, that the possible faults may have a regimen change.

The daily seismic activity registered in the PUMA station from 1/12/2009 to 31/5/2010 (Fig. 3b) shows a clear increase coincident with the $M_w = 8.8$ Maule earthquake, and also two local peaks associated with the $M_w = 4.5$ 2010/04/03 and $M_w = 3.9$ 2010/05/29 aftershocks (Table 1, Fig. 5). During the 88 days before the Maule earthquake, we measured 20 events, and during the subsequent 94 days we measured 188 quakes. This indicates that the seismicity of the area increased more than nine-fold. We localized 60 events during eight months between 2011 and 2012 (Table 2), indicating a decay in static stress changes. It must be taken into account that both earthquakes, the $M_w = 4.5$ 2010/04/03 and $M_w = 3.9$ 2010/05/29, have their own aftershocks which increase the total amount of earthquakes and they should be discarded. In order to differentiate the aftershocks form the rest of the regional seismicity, more precise locations would be required.

ISOLA software was used to obtain the seismic moment tensor (Table 2 and Appendix B) (Zahradnik et al., 2005; Sokos and Zahradnik, 2008). This software used a representation of multiple

Table 1
Locations and focal mechanisms obtained for the 2001/08/21, 2010/04/03, and 2010/05/29 Earthquakes.

Date	Time (UTM)	Long. (°W)	Lat. (°S)	Depth (km)	Mag.	HASH	ISOLA
2001/08/21	12:01	−70.340	−35.226	30.1	2.7 M_d	258/76/-60 11/33/-153	
NEIC		−70.39	−35.24	21	3.7 M_b		
2010/04/03	03:38	−70.371	−35.349	31	3.4 M_d	80/89/30	81/82/36
Centroid		−70.371	−35.354	40	4.5 M_w	349/60/179	345/54/170
NEIC		−70.34	−35.32	6	4.4 M_b		
2010/05/29	17:15	−70.488	−35.355	20.7	3.0 M_d	36/37/-24	49/62/-12
Centroid		−70.499	−35.356	4	3.9 M_w	146/76/-124	145/79/-151
NEIC		−70.26	−35.45	10	4.1 M_b		

sources, and an iterative deconvolution based in the method proposed by Kikuchi and Kanamori (1991). P-wave first motion focal mechanisms were resolved using HASH (Hardebeck and Shearer, 2002).

The stress variation calculations in the arc region (Fig. 6) were performed using Coulomb criterion with Coulomb 3.2 software (Toda et al., 2005; Lin and Stein, 2004). In our case the Maule, $M_w = 8.8$, 2/27/2010, Chile, is the source earthquake. Its location, the focal mechanism and the slip distribution were obtained from USGS (http://earthquake.usgs.gov/earthquakes/eqinthenews/2010/us2010tfan/).

5. Stress variation and seismicity activation in Andean arc region

The seismicity detected by PUMA station during 2009–2010 is mainly concentrated between 35°S and 36°S, near the international Argentinean–Chilean border (Figs. 4 and 5). The pre-Maule seismicity was scattered within the area (green circles in Fig. 4). During the post-Maule events two trends of seismicity were observed. To the north of the Planchón-Peteroa volcano, a NNE strip of seismicity is observed, while to the south of it, seismicity is concentrated along a NNW strip, in accordance with the observed seismicity of Rietbrock et al. (2012).

Our 2011–2012 seismicity location shows a similar pattern, with a concentration along the northern NNE-trending segment (violet circles in Fig. 4).

The increase in seismicity registered in the arc region since the occurrence of the Maule earthquake (Fig. 2) suggests causal relation between the mega-thrust earthquake and seismicity in the arc region.

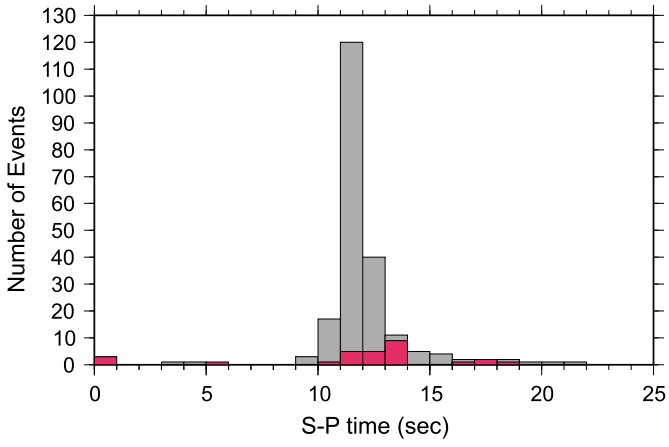

Fig. 2. S–P time histograms from different time periods, 88 days before the $M_w = 8.8$ Maule earthquake occurrence (in red) and 94 days after the quake (in gray). This last period includes 15 days without data (see Fig. 3b). In the analysis we do not consider recorded data with S–P≥19 s. Note that seismicity increased by more than nine times after the great earthquake. (For interpretation of the references to color in this figure legend, the reader is referred to the web version of this article.).

We investigated the plausibility of this relation, calculating the stress variation in the arc caused by the Maule earthquake as a fault source.

Near the activated seismicity zone, Folguera et al. (2006) propose the existence of Las Loicas trough by tectonic considerations, though there are no clear superficial evidences of them. The proposed fault coincides with the earthquake strip found and because of this we studied its possible activation. We also chose the most important structures of the arc, the 80° west-dipping N to NNE-trending La Gloria fault; the 75° west-dipping NNE-trending Río del Cobre fault; and the 60° west-dipping, NNW-trending Río Grande fault (Fig. 1), as well as the subvertical WNW lineaments (Table 3). We perform calculations on them at 5 km depth, and

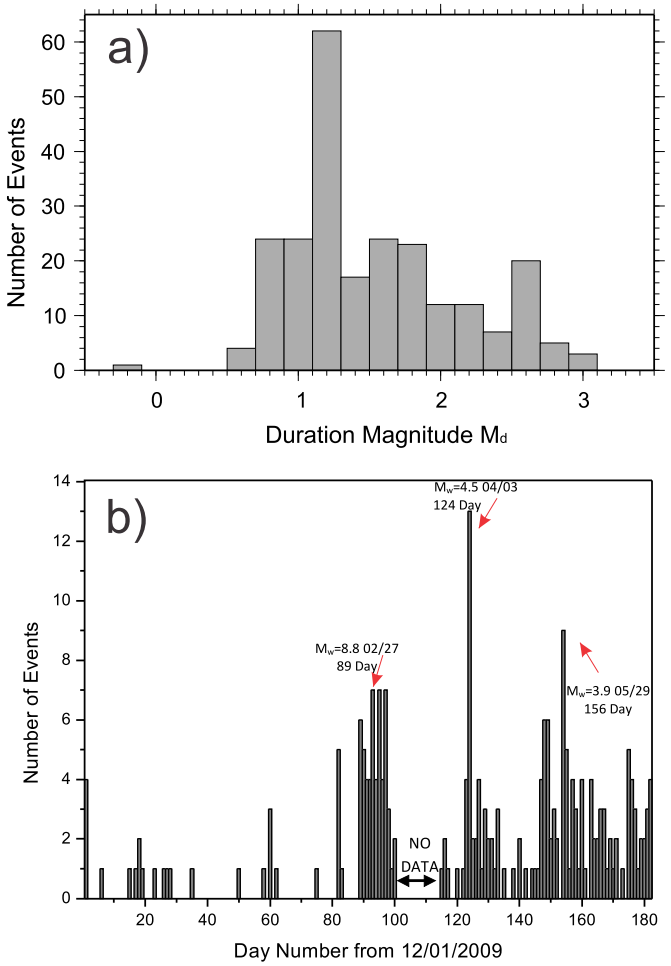

Fig. 3. a) Histogram showing magnitudes for the 2009–2010 events. b) Earthquake counting detected at PUMA station from 12/1/2009 to 5/31/2010. There is a clear seismicity increase on the day of the $M_w = 8.8$ Maule Earthquake occurrence (day 89), and in the other peaks related to the $M_w = 4.5$ and $M_w = 3.9$ earthquakes. Note the "NO DATA" gap due to ill recording.

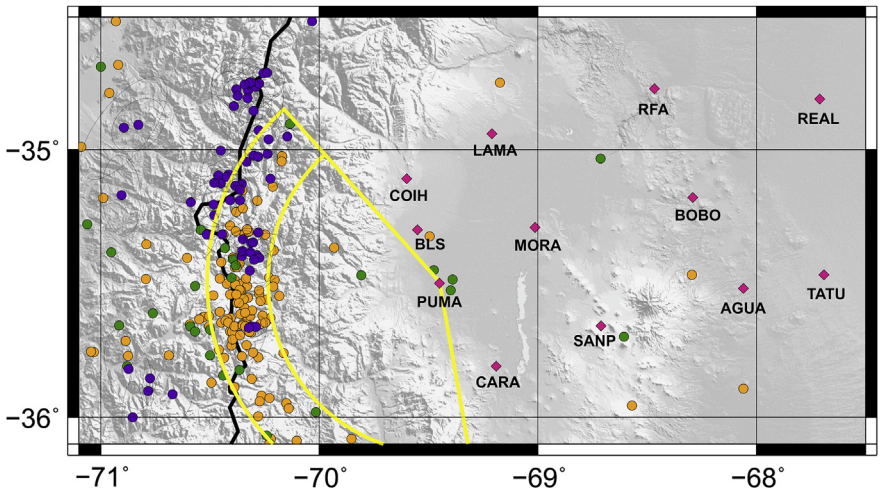

Fig. 4. San Rafael Block network: Fuchsia diamonds indicate location of seismological stations. Green and orange dots show seismicity recorded by the PUMA station, correspond to quakes occurred during the 88 and 94 day periods before and after the Maule quake, respectively. Circular sectors, in yellow, show anomalous azimuthal dispersion locations. Violet dots indicate the recorded seismicity in the shown network between 2011 and 2012. Fine black lines show error ellipses for these quakes. Solid black line: Argentina and Chile political boundary. Topography is taken from Shuttle Radar Topography Mission. (For interpretation of the references to color in this figure legend, the reader is referred to the web version of this article.).

tested different fault types: reverse, normal, strike-slip, normal/strike-slip and reverse/strike-slip. We observe that the more favorable movements correspond to dextral/normal movement ($\lambda \sim -130^{\circ}$) along the N–S and NNW-trending faults, in agreement with the 145/79/-151 nodal plane of the M = 4.1 earthquake mechanism. Therefore, we suggest that the post-Maule seismicity is associated to the reactivation of the La Gloria and Río Grande faults with transtensional movements. As expected, the modeling of the inverse fault planes indicates that they are unfavorable for the seismicity activation. The small stress changes triggered by the mega earthquake suggest that these NNE-striking, subvertical faults correspond to active strike-slip structures in critical state of incipient failure. In this regard, the static change in stress only modified the normal stress active on these faults, allowing them to failure with a normal/strike-slip movement.

The calculations shown in Table 3 indicate that the normal component of the stress $\mu'\Delta\sigma_n$ is bigger than the shear component $\Delta\tau_s$, suggesting that the unclamping is the predominant mechanism for the seismicity activation in every case. In the NNW-trending plane, the normal stress component (258° azimuth) coincides with the co-seismic extension direction determined by GPS in the region (Vigny et al., 2011; Delouis et al., 2010; Pollitz et al., 2011; Lorito et al., 2011; Moreno et al., 2012). Extrapolation of the GPS measurements indicates ~40–55 cm of co-seismic horizontal displacement towards the west in the arc region with respect to 30 mm of co-seismic displacement to the 60°W (Pollitz et al., 2011). This orientation is perpendicular to the NNW inferred structures, and has clearly favored a predominant normal component of slip.

We also evaluated variations in the effective friction coefficient μ'. The calculation of the static stress change using different μ' values (between 0.4 and 0.8) show variations of less than 1 bar in the results, suggesting that the pre-existing plane properties do not play a fundamental role in the unclamping process.

Parsons et al. (1999) found that high shear stress changes were correlated with seismicity-rate increases on major, high-angle, strike-slip faults with low value of effective friction, while high normal (unclamping) stress changes were significantly correlated with seismicity-rate increases on oblique (right-lateral/thrust) faults with high value of friction. These authors also suggest that the presence of fluids trapped in the pores would increase the normal stress change influence, explaining why intermediate coefficients of friction may be used to describe the correspondence of Coulomb stress changes to aftershock distributions in regions that contain both types of faults, such as our analyzed area.

King et al. (1994) show that Coulomb stress changes in the upper crust may increase as a result of stress relaxation processes over long time periods.

We claim that the small static stress changes are not capable of changing the tectonic regime and major faults behavior though they would temporally favor the seismicity-rate increase on dextral normal/strike-slip faults.

6. Discussion

The present-day tectonic activity in the Andean volcanic arc between 35° and 36°S is a matter of debate. At these latitudes, some authors propose compressional tectonics, while others propose extension and even strike-slip tectonics. The NNW seismically active strip determined in this study coincides with the Río Grande valley. This region has previously been assigned by Folguera et al. (2006) and Ramos and Kay (2006) to a tectonic depression, named Las Loicas trough, inferred by these authors to be active since the Late Pliocene up to present under an extensional stress field. Folguera et al. (2006, 2008) interpreted the presence of a half-graben controlled by a west-dipping NNW-trending normal fault. They based this interpretation in a northward prolongation of the quaternary extensional depocenters. Immediately to the west of the Las Loicas trough, the Novillo and Calabozos faults have been considered reverse, the last one yielding evidence of Quaternary activity (Tapia et al., 2015). On the other hand, seismicity with strike-slip mechanisms has been associated with movement along NNE-trending dextral strike-slip faults (Farías, 2007; Comte et al., 2008), such as the 2004 and 2012 earthquakes.

The increase in seismicity ($M_d < 3.1$) after the Maule earthquake is concentrated along the NNW to NNE trending inferred structures, which includes the Pleistocene volcanic centers: Calabozos, Puelche and Maule. We investigated the plausibility of the three tectonic settings by modeling the inferred NNW-, N- and NNE-trending receiver fault as a (a) normal, (b) reverse, and (c) strike-slip fault, and the Maule earthquake as a source. By modeling the nearby reverse faults we observed that the stress variation has not

Table 2
2011–2012 Earthquakes: Localization using hypocenter and velocity model Spagnotto (2013). (April and December 2011 and May to October 2012).

Year	Month/Date	HRMM	Sec	Latitud	Longitud	Depth	N of stations	RMS	Md
2011	4/1	1138	11	−35.046	−70.333	19.7	4	0	2.2
2011	4/7	638	26.2	−35.198	−70.588	12.4	4	0.3	2
2011	4/9	946	56.3	−35.399	−70.354	17	4	0.1	1.9
2011	4/10	507	2.4	−35.023	−70.300	22.5	4	0.1	2.2
2011	4/18	206	4.8	−35.454	−70.317	14.2	4	0.5	1.5
2011	12/5	727	38.1	−34.951	−70.147	23.4	6	0.3	2
2011	12/6	415	49.9	−35.128	−70.450	16.9	4	0.5	1.3
2011	12/8	1002	43.2	−35.396	−70.286	26.5	6	0.6	1.3
2011	12/14	712	57	−35.381	−70.352	25	5	0.5	1.4
2011	12/18	1909	58.2	−35.027	−70.280	11.8	5	0.4	1.7
2011	12/19	339	46.6	−35.916	−70.672	0	4	0.4	1.8
2011	12/19	940	0	−35.857	−70.775	0	4	0.1	2.1
2011	12/20	2212	3.6	−35.903	−70.783	5.8	4	0	1
2011	12/24	519	43	−35.385	−70.315	10.8	5	0.2	1.5
2011	12/27	812	30.9	−35.336	−70.350	32.3	4	0.3	1.2
2012	5/2	1514	39.7	−34.773	−70.380	2.1	7	0.7	2.1
2012	5/4	1424	46.3	−34.777	−70.327	10.8	5	0.9	2.3
2012	5/4	1408	25.9	−34.806	−70.328	3.1	7	0.8	2.1
2012	5/4	1827	32.5	−34.712	−70.256	9.2	6	0.6	2.2
2012	5/5	1620	49.3	−34.797	−70.374	9.2	5	0.9	1.8
2012	5/8	431	11.8	−34.917	−70.895	0	6	0.8	2.7
2012	5/8	601	34.2	−34.749	−70.323	10	6	0.8	2.1
2012	5/9	1954	11.4	−34.764	−70.290	12.4	6	1	2.1
2012	5/12	57	20.8	−34.710	−70.238	12.4	5	0.3	2.1
2012	5/23	1424	10.5	−34.752	−70.275	12.8	7	0.8	2.2
2012	5/24	45	46	−35.129	−70.355	11.3	7	0.3	2.5
2012	5/31	344	6.3	−35.136	−70.385	8.5	6	0.2	2.2
2012	5/31	1053	56.3	−35.152	−70.363	12.1	7	0.2	2.6
2012	6/7	856	27.5	−35.351	−70.311	17.4	6	0.6	2.5
2012	6/7	856	27.6	−35.349	−70.303	12.7	6	0.2	2.5
2012	6/11	2355	14	−35.407	−70.276	0	6	0.9	1.6
2012	6/12	1253	16.5	−35.318	−70.516	17.6	4	0.3	3.2
2012	6/14	855	28.3	−36.000	−70.854	4.7	5	0.3	2.9
2012	6/15	1057	23.2	−34.961	−70.232	18.2	6	0.6	2.1
2012	6/15	1406	26.4	−35.311	−70.279	3.6	5	0.1	2.3
2012	6/20	107	48.4	−35.319	−70.444	12.8	6	0.6	3.2
2012	6/22	919	53.8	−34.928	−70.277	17.4	5	0.6	2.4
2012	6/30	806	3.9	−35.662	−70.310	1.5	6	0.4	2.2
2012	6/30	806	4.2	−35.664	−70.290	0	6	0.3	2.5
2012	6/30	953	13.4	−35.667	−70.322	8.3	5	0.5	3.8
2012	7/15	1517	54.9	−34.907	−70.827	0	4	0.7	–
2012	7/18	645	40.7	−34.516	−70.033	3.8	4	0.2	–
2012	8/4	1502	1.6	−35.822	−70.873	3.9	6	0.3	2.2
2012	8/7	805	28.4	−34.746	−70.314	6.2	5	0.1	1.7
2012	8/13	2328	13.3	−35.172	−70.905	0	5	0.2	1.4
2012	8/25	122	49.1	−35.206	−70.482	13.4	8	0.8	1.6
2012	8/25	133	4.2	−35.190	−70.407	2.5	8	0.4	1.8
2012	8/27	2347	38.9	−35.414	−70.298	13.2	9	0.4	1.7
2012	8/30	129	41.8	−35.003	−70.451	10.1	5	0.2	1.5
2012	9/1	707	54.7	−35.098	−70.461	8.3	4	0.2	1.5
2012	9/9	609	36.5	−35.110	−70.223	26.7	6	0.3	1.9
2012	9/12	719	31.4	−34.754	−70.341	10.3	4	0.4	1.4
2012	9/14	1626	56.3	−35.017	−70.236	11	6	0.2	2.1
2012	9/19	1735	5.3	−34.854	−70.300	15.9	6	0.4	2
2012	9/24	315	18.2	−34.836	−70.391	17.3	5	0.6	1.9
2012	9/29	826	4.4	−35.126	−70.481	14.5	5	0.3	1.6
2012	9/30	1150	39.5	−35.094	−70.415	17.7	5	0.5	1.5
2012	10/6	455	47.1	−35.102	−70.422	17.7	5	0.3	1.6
2012	10/13	211	16.5	−35.247	−70.481	20.5	7	0.6	1.8
2012	10/19	325	58.9	−35.190	−70.362	31.1	4	0.1	1.4

been favorable for seismicity activation. Therefore, our results indicate that the stress variation becomes maximized for $\lambda \sim -130°$, involving significant normal right-lateral slip components along the inferred NNW to N–S trending structures. Therefore, the stress regime would tend to be strike-slip, with SW-oriented σ_1 and NW-oriented σ_3, in the arc region. Only due to the unclamping produced by the Maule earthquake could the regime have transitorily right lateral/normal component.

We performed calculations of Coulomb stress variation to analyze the possibility for the strike slip $M_w = 6.3$, 28/8/2004 earthquake to have influenced the stress regime. The rupture initiated near 35.2°S and spread toward north as the aftershocks found by Comte et al. (2008) and the slip distribution using inversion of teleseismic waves developed by Spagnotto (2013) suggest. We found that the stress variations inhibit the slip movement in the proposed receiver fault planes, thereby allowing them to discard a relationship between this earthquake and the analyzed seismicity.

The Peteroa volcano activation between September/6 and October/13 of 2010 (according to Global Volcanism Program),

Table 3
Stress variations on receiver fault planes with different dips and rakes.

Receiver fault plane strike/dip/rake: Φ/δ/λ (Aki and Richard, 1980, convention)		Calculations at 35.6°S, 70.46°W, depth = 5 km, μ′ = 0.6		
		Shear	Normal	Total
Strike equal to NNW seismicity strip (168° and 348° strike – Río Grande fault or Las Loicas tougth)	168/60/-90	2.414	4.692	5.229
	168/60/-130	2.949	4.692	5.764
	168/60/180	1.710	4.692	4.525
	168/60/90	−2.414	4.692	0.401
	168/60/0	−1.710	4.692	1.105
	168/60/-125	2.959	4.692	5.774
	168/70/0	−1.833	5.413	1.415
	168/70/-130	2.463	5.413	5.711
	168/70/-90	1.678	5.413	4.926
	168/50/-90	2.860	3.762	5.117
	348/60/-120	3.141	4.190	5.655
	348/60/-80	2.385	4.190	4.899
	348/60/90	−2.704	4.190	−0.19
	348/60/0	−1.598	4.190	0.916
	348/60/-125	3.132	4.190	5.646
	348/60/-90	2.704	4.190	5.218
	348/60/180	1.598	4.190	4.112
	348/70/-130	2.754	5.041	5.779
	348/70/90	−2.121	5.041	0.903
	348/70/0	−1.757	5.041	1.268
	348/70/-90	2.121	5.041	5.146
NNE fault (Rio del Cobre fault) considered as reverse, normal, left and right lateral	20/60/-90	2.930	4.554	5.662
	20/60/0	0.927	4.554	3.660
	20/60/180	−0.927	4.554	1.806
	20/60/-70	3.070	4.554	5.803
	20/60/-120	2.074	4.554	4.806
	20/60/90	−2.930	4.554	−0.197
N–S fault (La Gloria fault) considered as reverse, normal, left and right lateral	180/70/90	−1.854	5.945	1.713
	180/70/-90	1.854	5.945	5.421
	180/70/0	−0.831	5.945	2.736
	180/70/180	0.831	5.945	4.398
	180/60/180	0.775	5.149	3.864
	180/60/0	−0.775	5.149	2.314
	180/60/90	−2.661	5.149	0.428
	180/60/-90	2.661	5.149	5.751
	180/60/-120	2.692	5.149	5.782
WNW trending lineament considered as reverse, normal, left and right lateral	320/70/90	−1.240	2.857	0.474
	320/70/-90	1.240	2.857	2.955
	320/70/0	−2.606	2.857	−0.892
	320/70/180	2.606	2.857	4.321
	320/70/-150	2.877	2.857	4.591
	320/60/90	−1.563	2.363	−0.145
	320/60/-90	1.563	2.363	2.981
	320/60/0	−2.358	2.363	−0.94
	320/60/180	2.358	2.363	3.776
	320/60/-150	2.824	2.363	4.242
Faults like the nodal planes from focal mechanisms in Table 1	258/76/-60	1.199	1.558	2.134
	11/33/-153	1.214	1.690	2.228
	80/89/30	1.451	1.466	2.331
	349/60/179	1.486	4.237	4.029
	36/37/-24	2.218	1.706	3.242
	146/76/-124	2.196	3.859	4.512

Note: Calculations by Coulomb 3.2 software at 35.6°S, 70.46°W, depth = 5 km, μ′ = 0.6. Slip distribution on the M_w = 8.8, February 27, 2010, Maule, Chile, fault plane earthquake as source is taken from USGS. Hypocenter location: 35.85°S, 72.72°W; depth = 35 km. The fault plane is defined using the W-phase moment tensor solution of NEIC (strike = 16, dip = 14, rake = 104).

which is close to the northern end NNW strip (Fig. 1) may also be possibly related to the M_w = 8.8, 27/2/2010 Maule earthquake, as it has been suggested by Pritchard et al. (2013) and Bonali et al. (2013). These authors document N–S oriented subsidence of more than 10 cm in the Cerro Azul, as well as in the Calabozos volcanoes and less than 5 cm in Planchón-Peteroa volcano using INSAR and night-time thermal infrared data. They suggest that the Maule earthquake caused a region of east–west tension in the surrounding of the subsiding volcanoes, provoking the release of hydrothermal fluids, increased streamflow and ground deformation. Even though these authors inferred that the deformation was mostly aseismic, the seismicity analyzed in this paper shows activity in the region of subsidence.

In long term periods, after mega-thrust earthquakes, Lupi and Miller (2014) analyzed the eruptive increase in volcanic arcs, using geomechanical, geological, and geophysical arguments, and conclude that this increment is due to the relaxation of the compressional regime. The reduction of the horizontal stress would favor magma mobilization and strike-slip faulting. In particular, Lupi and Miller (2014), analyzed the Mw 8.8 2010 Maule, Chile earthquake and other 4 mega earthquakes. They found that the consequent shallow earthquakes show a marked lateral component. The onset of strike-slip faulting is controlled by (i) the degree

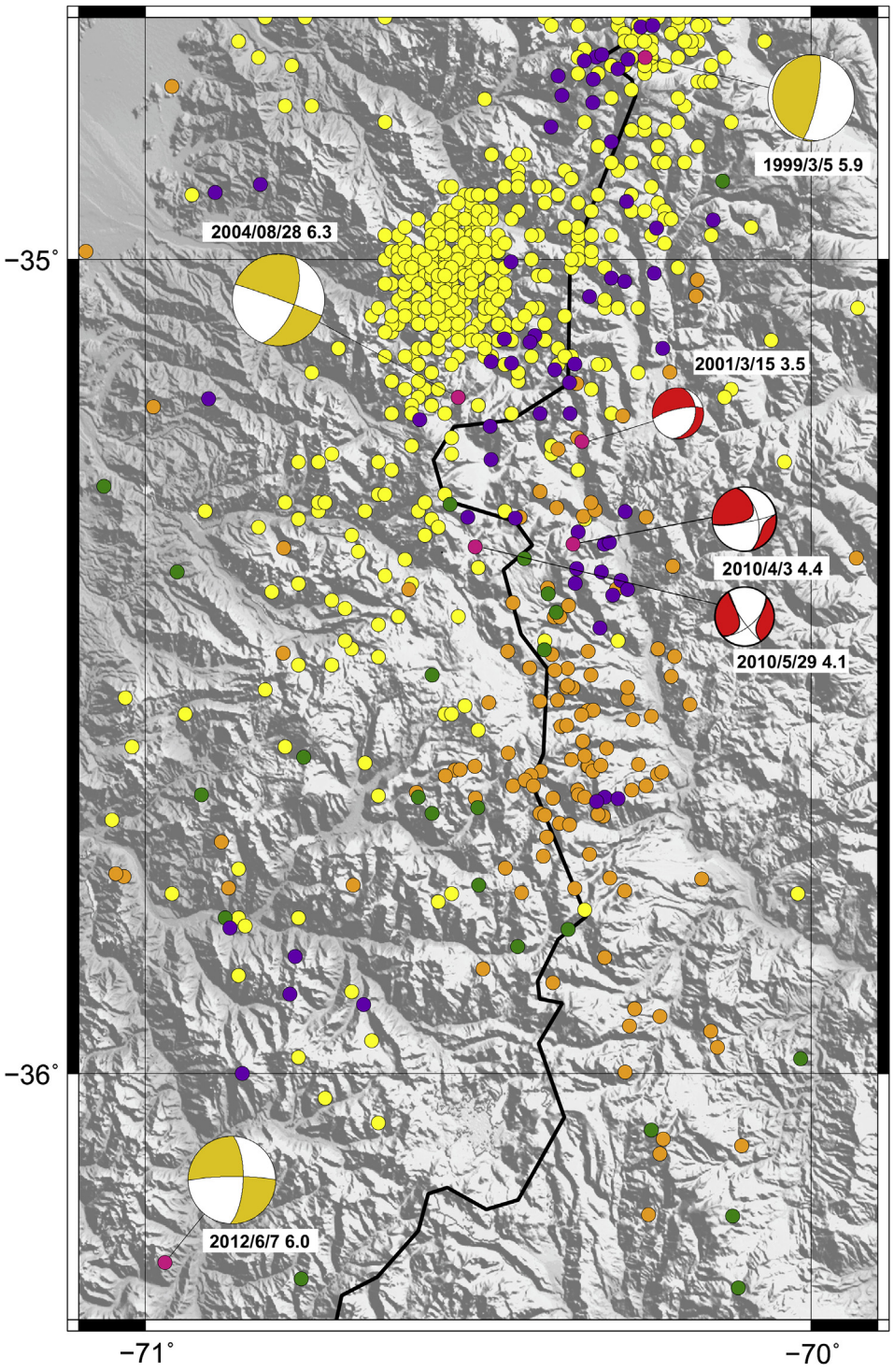

Fig. 5. Crustal earthquakes and focal mechanisms in the arc region. Epicenters shown by circles: yellow ones are from NEIC (USGS) from 1990 to $M_w = 8.8$ Maule earthquake, green and orange circles are earthquakes located using PUMA station data before and after the $M_w = 8.8$ earthquake, respectively. Epicenters are shown with fuchsia circles and their corresponding focal mechanisms with red beach balls (lower hemisphere compressional quadrants) for our solutions (Table 1) and dark yellow ones for CMT solutions (Centroid Moment Tensor, Harvard). Scaled to the magnitude are all focal spheres. Topography is taken from Shuttle Radar Topography Mission. (For interpretation of the references to color in this figure legend, the reader is referred to the web version of this article.).

of strain partitioning at convergent margins, (ii) the inter-seismic duration that controls the shear stress amplitudes, and (iii) the relative values of the vertical and horizontal principal stresses before the mega-thrust earthquake.

The degree of strain-partitioning strongly affects the switch from reverse to strike-slip environments (Chemenda et al., 2000).

7. Conclusions

The $M_w = 8.8$, 2/27/2010 Maule earthquake occurrence increased more than nine times the seismicity in a narrow longitudinal Andean area, between 35°S and 36°S. The magnitudes M_d found are $\leq$3.1, except for two earthquakes with M_w 3.9 and 4.5 at

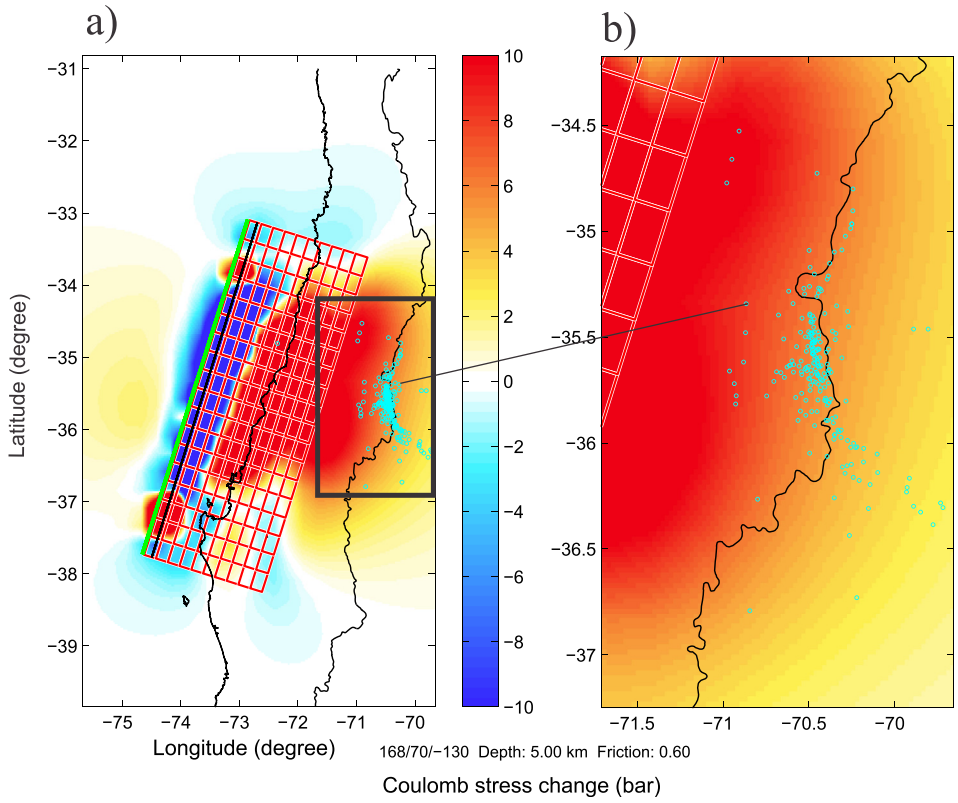

Fig. 6. Coulomb stress change calculated with Coulomb 3.2 software. Fault plane earthquake source was taken from slip distribution on the $M_w = 8.8$, February 27, 2010, Maule, Chile, reported by USGS. Receiver fault plan is 168/70/-130 (normal component coincident with GPS measurements). Seismicity shown as light blue circles. a) Regional view b) Zoom indicated in figure a). (For interpretation of the references to color in this figure legend, the reader is referred to the web version of this article.).

~35.3°S. We model the stress variation in the NNW- and NNE-trending area caused by the slip distribution on the Maule fault plane, assuming NNW, N–S and NNE oriented receiver planes with dips of 60°, 80° and 80° respectively. The stress variation becomes maximized for slip $\lambda \sim -130°$ for both east- and west-dipping planes, suggesting significant normal/right lateral slip components.

The amount of normal component in stress variation is bigger than the shear one, allowing us to propose that the unclamping is the predominant mechanism for the seismicity activation. Notably, the normal stress component (258° azimuth), coincides with the co-seismic extension direction determined by GPS in the region, strengthening the working hypothesis.

Previous works propose three different Quaternary tectonic settings-extensional, strike-slip and compressional-for the region. We found that the most favorable one is the strike-slip regime, and only due to the unclamping produced by the Maule earthquake could the regime have transitorily changed to a right lateral/normal regime. This unclamping of pre-existing faults could have generated slip along them, promoting the observed subsidence in the nearby volcanoes due to magma migration.

Acknowledgments

We would like to thank the Pierre Auger Observatory and the Instituto Nacional de Previsión Sísmica (INPRES), Argentina as well as the IRIS Data Management Center (USA) for the waveforms obtained. Our research was founded by PICTO N°254 Riesgo Sísmico, 2011–2014 and PICT-2011-1079.

Appendix A

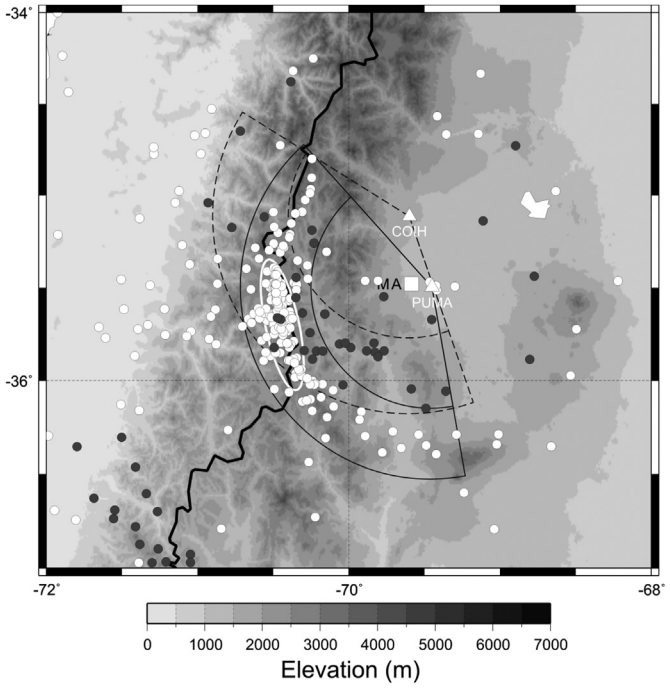

Seismicity recorded by stations PUMA (white circles) and COIH (gray dark circles) within the same period as in Fig. 2. Circular sectors, corresponding to each one of the two stations, show anomalous azimuthal dispersion locations (as a consequence of the location procedure by only one station). The circumferences radius are distances to the station between about 92 and 110 km. Assuming Vp~6 km/s these values implies $11 \leq$ S–P times <19 s for rays leaving de source at cero depth. White ellipse: best earthquake locations. MA: Malargüe City (White Square). Solid black line: Argentina and Chile political boundary. Topography: scale in meters.

Appendix B

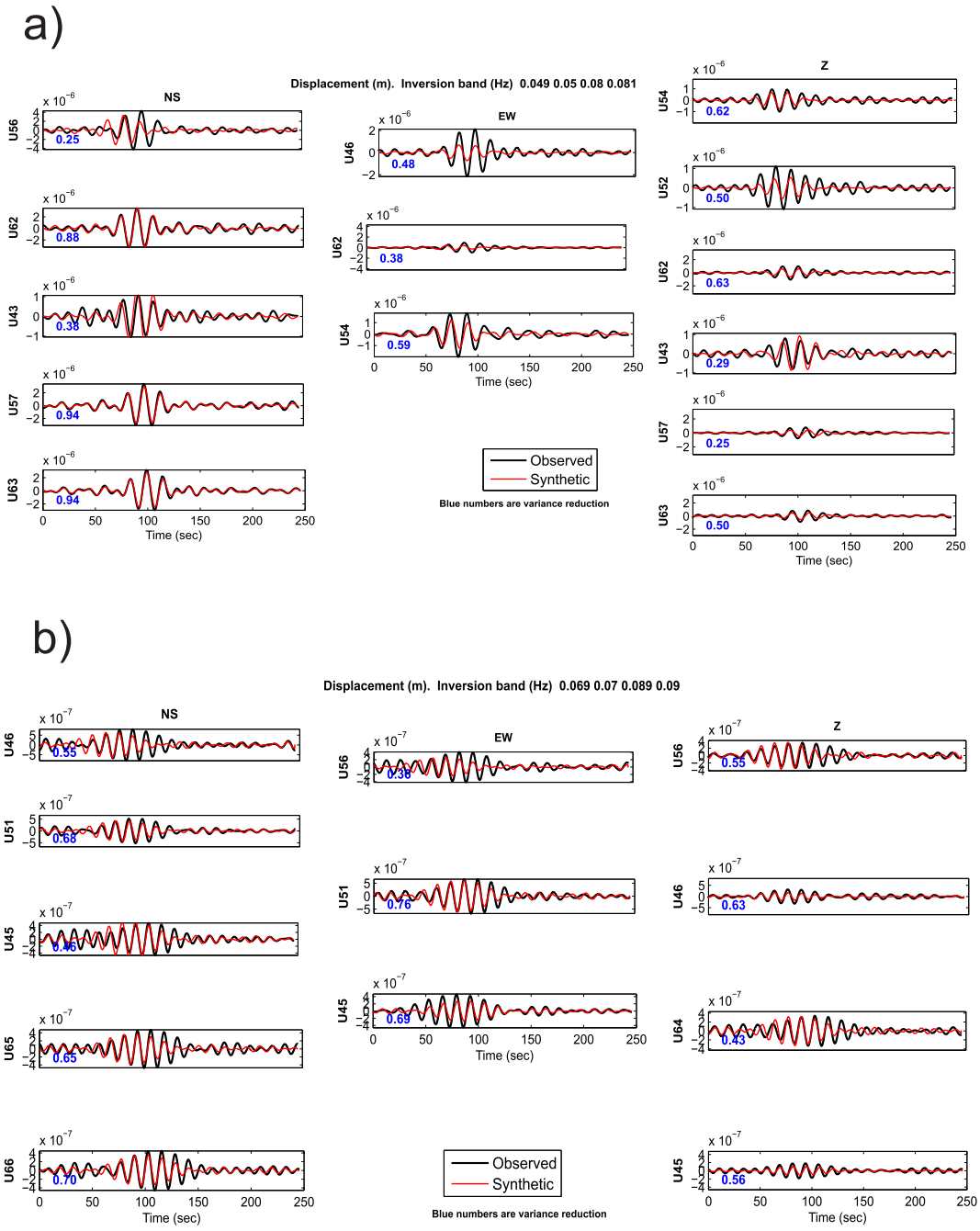

Observed waveforms (black) and synthetic (red) used in the ISOLA software inversion. On the left sides are the names of the implemented stations. Columns correspond to N–S, E–W and vertical components. In blue is indicated the reduction variance: A) 2010/04/03 earthquake, and B) 2010/05/29 earthquake.

References

Aki, K., Richards, P.G., 1980. Quantitative Seismology. Freeman and Co., New York.

Anderson, J.G., Brune, J.N., Louie, J.N., Zeng, Y.H., Savage, M., Yu, G., Chen, Q., dePolo, D., 1994. Seismicity in the western Great Basin apparently triggered by the Landers, California, earthquake 28 June 1992. Bull. Seismol. Soc. Am. 84, 863–891.

Anderson, M.L., Alvarado, P., Zandt, G., Beck, S., 2007. Geometry and brittle deformation of the subducting Nazca Plate Central Chile and Argentina. Geophys. J. Int. 171, 419–434.

Aron, F., Allmendinger, R.W., Cembrano, J., González, G., Yáñez, G., 2013. Permanent forearc extension and seismic segmentation: insights from the 2010 Maule earthquake, Chile. J. Geophys. Res. http://dx.doi.org/10.1029/2012JB009339.

Bak, P., Tang, C., 1989. Earthquakes as a self-organized critical phenomenon. J. Geophys. Res. 94 (B11), 15635–15637. http://dx.doi.org/10.1029/JB094iB11p15635.

Barrientos, S., Vera, E., Alvarado, P., Monfred, T., 2004. Crustal seismicity in central Chile. J. South Am. Earth Sci. 16, 759–768.

Bechis, F., Giambiagi, L., García, V., Lanés, S., Cristallini, E., Tunik, M., 2010. Kinematic analysis of a transtensional fault system: the Atuel depocenter of the Neuquén basin, southern Central Andes, Argentina. J. Struct. Geol. 32, 886–899.

Belardinelli, M.E., Bizzarri, A., Cocco, M., 2003. Earthquake triggering by static and dynamic stress changes. J. Geophys. Res. 108 http://dx.doi.org/10.1029/2002JB001779.
Bonali, F.L., Tibaldi, A., Corazzato, C., Tormey, D.R., Lara, L.E., 2013. Quantifying the effect of large earthquakes in promoting eruptions due to stress changes on magma pathway: the Chile case. Tectonophysics 583, 54–67.
Byerlee, J.D., 1978. Friction of rocks. Pure Appl. Geophys. 116, 615–626.
Cembrano, J., Lara, L., 2009. The link between volcanism and tectonics in the southern volcanic zone of the Chilean Andes: a review. Tectonophysics 471, 96–113.
Charrier, R., Baeza, O., Elgueta, S., Flynn, J.J., Gans, P., Kay, S.M., Muñoz, N., Wyss, A.R., Zurita, E., April 2002. Evidence for Cenozoic extensional basin development and tectonic inversion south of the flat-slab segment, southern Central Andes, Chile (33°–36°S.L). J. South Am. Earth Sci. Flat-Slab Subduction Andes 15 (1), 117–139.
Chemenda, A., Lallemand, S., Bokun, A., 2000. Strain partitioning and interplate friction in oblique subduction zones – constraints provided by experimental modeling. J. Geophys. Res. 105, 5567–5581.
Comte, D., Farías, M., Charrier, R., González, A., 2008. Active tectonics in the Central Chilean Andes: 3D tomography based on the aftershock sequence of the 28 August 2004 shallow crustal earthquake. In: 7th International Symposium on Andean Geodynamics (ISAG 2008, Nice), Extended Abstracts, pp. 160–163.
Cowie, P.A., Vanneste, C., Sornette, D., 1993. Statistical physics model for the spatiotemporal evolution of faults. J. Geophys. Res. 98 (B12), 21809–21821.
Delouis, B., Nocquet, J.M., Vallée, M., 2010. Slip distribution of the February 27, 2010 $M_w = 8.8$ Maule earthquake, central Chile, from static and high rate GPS, InSAR, and broadband teleseismic data. Geophys. Res. Lett. 37, L17305. http://dx.doi.org/10.1029/2010GL043899.
Douglas, A., 1967. Join hypocenter determination. Nature 215, 47–48.
Farías, M., 2007. Tectonique, érosion et évolution du relief dans les Andes du Chili Central au cours du Néogene (Ph.D. thesis). Universite Toulouse III – Paul Sabatier UFR Sciences de la Vie et la Terre.
Farías, M., Comte, D., Roecker, S., Carrizo, D., Pardo, M., 2011. Crustal extensional faulting triggered by the 2010 Chilean earthquake: the Pichilemu seismic sequence. Tectonics 30. http://dx.doi.org/10.1029/2011tc002888 tc6010, 11 pp.
Folguera, A., Espinach, S., Utge, S., Rojas Vera, E., Ramos, V.A., 2005a. Evolución Tectónica de los Andes entre 36° y 38°S. 16° Congreso geológico Argentino, Actas, Tomo, vol. 2, pp. 19–22 (La Plata).
Folguera, A., Ramos, V.A., Zapata, T., Spagnuolo, M., Miranda, F., 2005b. Pliocene to Quaternary retro-arc extensión in the Andes at 35°–37° 30′S. In: 6th International Symposium on Andean Geodynamics, Extended Abstracts, pp. 277–280.
Folguera, A., Zapata, T., Ramos, V.A., 2006. Late Cenozoic Extension and the Evolution of the Neuquén Andes. Evolution of the Andean Margin: a Tectonic and Magmatic View from the Andes to the Neuquén Basin (35°–39°S Latitude). In: Geological Society of America Special Paper, vol. 407, pp. 267–285.
Folguera, A., Bottesi, G., Zapata, T., Ramos, V.A., 2008. Crustal collapse in the Andean back-arc since 2 Ma: Tromen volcanic plateau, southern Central Andes (36°40′–37°30′S). Tectonophysics 459 (1–4), 140–160. http://dx.doi.org/10.1016/j.tecto.2007.12.013 (Special Issue Andean Geodynamics.
Freed, A., 2005. Earthquake triggering by static, dynamic, and postseismic stress transfer. Annu. Rev. Earth Planet. Sci. 33, 335–367. http://dx.doi.org/10.1146/annurev.earth.33.092203.122505.
Giambiagi, L.B., Bechis, F., García, V., Clark, A., 2008. Temporal and spatial relationship between thick- and thin-skinned deformation in the Malargüe fold and thrust belt, southern Central Andes. Tectonophysics 459, 123–139.
Giambiagi, L., Ghiglione, M., Cristallini, E., Bottesi, G., 2009. Kinematic models of basement/cover interaction: insights from the Malargüe fold and thrust belt, Mendoza, Argentina. J. Struct. Geol. 31, 1443–1457.
Godoy, E., Yáñez, G., Vera, E., 1999. Inversion of an Oligocene volcano-tectonic basin and uplifting of its superimposed Miocene magmatic arc in the Chilean Central Andes: first seismic and gravity evidences. Tectonophysics 306, 217–236.
Gomberg, J., Bodin, P., Reasenberg, P.A., 2003. Observing earthquakes triggered in the near field by dynamic deformations. Bull. Seismol. Soc. Am. 93, 118–138.
Haller, M.J., Risso, C., 2011. La erupción del volcán Peteroa (35°15′S, 70°18′O) del 4 de septiembre de 2010. Rev. Assoc. Geol. Argent. 68 (2).
Hardebeck, J.L., Shearer, P.M., 2002. A new method for determining first motion focal mechanisms. Bull. Seismol. Soc. Am. 92, 2264–2276.
Hill, D.P., Reasenberg, P.A., Michael, A.J., Arabasz, W.J., Beroza, G.C., 1993. Seismicity remotely triggered by the magnitude 7.3 Landers, California earthquake. Science 260, 1617–1623.
Jay, J.A., Pritchard, M.E., West, M.E., Christensen, D., Haney, M., Minaya, E., Sunagua, M., McNutt, S.R., Zabala, M., 2012. Shallow seismicity, triggered seismicity, and ambient noise tomography at the long-dormant Uturuncu Volcano, Bolivia. Bull. Volcanol. 74, 817–837.
Kikuchi, M., Kanamori, H., 1991. Inversion of complex body waves III. Bull. Seismol. Soc. Am. 81, 2335–2350.
Kilb, D., Gomberg, J., Fodin, P.B., 2002. Aftershock triggering by complete Coulomb stress changes. J. Geophys. Res. 107 (B4) http://dx.doi.org/10.1029/2001JB000202.
King, G.C.P., Stein, R.S., Lin, J., 1994. Static stress changes and the triggering of earthquakes. Bull. Seismol. Soc. Am. 84 (3), 935–953.
Kozlowski, E.E., Manceda, R., Ramos, V.A., 1993. Estructura, in Geología y Recursos Naturales de Mendoza, XII Congreso Geologico Argentino y II Congreso Explor. Hidrocarburos. In: Ramos, V.A. (Ed.), Relatorio, vol. I(18), pp. 235–256 (Mendoza, Argentina).
Lange, D., Tilmann, F., Barrientos, S., Contreras-Reyes, E., Methe, P., Moreno, M., Heit, B., Agurto, H., Bernard, P., Vilotte, J.P., Beck, S., 2012. Aftershock seismicity of the 27 February 2010 Mw 8.8 Maule earthquake rupture zone. Earth Planet. Sci. Lett. 317–318, 413–425.
Lienert, B.R., Berg, E., Frazer, N., 1986. Hypocenter: an earthquake location method using centered, scaled, and adaptively damped least squares. Bull. Eeismol. Soc. Am. 76 (3), 771–783.
Lienert, B.R.E., Havskov, J., 1995. A computer program for locating earthquakes both locally and globally. Seismol. Res. Lett. 66, 26–36.
Lin, J., Stein, R.S., 2004. Stress triggering in thrust and subduction earthquakes, and stress interaction between the southern San Andreas and nearby thrust and strike-slip faults. J. Geophys. Res. 109, B02303. http://dx.doi.org/10.1029/2003JB002607.
Lira Martinez, E.S., 2011. Estudio de sismicidad, tomografía sísmica y modelo de física de rocas: potencial sistema geotermal asociado al complejo volcánico Tinguiririca (Magister thesis). Universidad de Chile.
Lorito, S., Romano, F., Atzori, S., Tong, X., Avallone, A., McCloskey, J., Cocco, M., Boschi, E., Piatanesi, A., 2011. Limited overlap between the seismic gap and coseismic slip of the great 2010 Chile earthquake. Nat. Geosci. http://dx.doi.org/10.1038/ngeo1073, 1752–0908.
Lupi, M., Miller, S.A., 2014. Short-lived tectonic switch mechanism for long-term pulses of volcanic activity after mega-thrust earthquakes. Solid Earth 5, 13–24. http://dx.doi.org/10.5194/se-5-13-2014.
Manceda, R., Figueroa, D., 1995. Inversion of the Mesozoic Neuquén rift in the Malargüe fold thrust belt, Mendoza, Argentina. In: Tankard, A.J., Suarez, R., Welsink, J. (Eds.), Petroleum Basin of South America. American Association of Petroleum Geologist, Volume Memoir, pp. 369–382.
Mescua, J.F., Giambiagi, L.B., Ramos, V.A., 2013. Late Cretaceous Uplift in the Malargüe fold-and-thrust belt (35°S), southern Central Andes of Argentina and Chile. Andean Geol. 40 (1), 102–116. http://dx.doi.org/10.5027/andgeoV40n1-a05.
Moreno, M., Melnick, D., Rosenau, M., Baez, J., Klotz, J., Oncken, O., Tassara, A., Chen, J., Bataille, K., Bevis, M., Socquet, A., Bolte, J., Vigny, C., Brooks, B., Ryder, I., Grund, V., Smalley, B., Carrizo, D., Bartsch, M., Hase, H., 2012. Toward understanding tectonic control on the Mw 8.8 2010 Maule Chile earthquake. Earth Planet. Sci. Lett. 321–322, 152–165. http://dx.doi.org/10.1016/j.epsl.2012.01.006.
Ottemöller, L., Voss, P.H., Havskov, J., 2012. SEISAN: Earthquake Analysis Software for Windows, Solaris, Linux and Macosx. ftp://ftp.geo.uib.no/pub/seismo/SOFTWARE/SEISAN/seisan.pdf.
Parada, R., 2008. Análisis estructural del borde oriental de la cuenca terciaria de Abanico en la valle del Río Teno, 7ma región (Thesis to obtein the degree of geology). Facultad de Ciencias Físicas y Matemáticas. Universidad de Chile.
Parsons, T., Stein, R.S., Simpson, R.W., Reasenberg, P.A., 1999. Stress sensitivity of fault seismicity: a comparison between limited-offset oblique and major strike-slip faults. J. Geophys. Res. 104, 20,183–20,202.
Peng, Z., Hill, D.P., Shelly, D.R., Aiken, C., 2010. Remotely triggered microearthquakes and tremor in central California following the 2010 Mw 8.8 Chile earthquake. Geophys. Res. Lett. 37, L24312. http://dx.doi.org/10.1029/2010GL045462.
Piquer, J., Castelli, J.C., Charrier, R y, Yañez, G., 2010. El Cenozoico del alto río Teno, Cordillera principal, Chile Central: estratigrafía, plutonismo y su relación con estructuras profundas. Andean Geol. 37 (1), 32–53.
Pollitz, F.F., Brooks, B., Tong, X., Bevis, M.G., Foster, J.H., Bürgmann, R., Smalley Jr., R., Vigny, C., Socquet, A., Ruegg, J.C., Campos, J., Barrientos, S., Parra, H., Baez Soto, J.C., Cimbaro, S., Blanco, M., 2011. Coseismic slip distribution of the February 27, 2010 Mw 8.8 Maule, Chile earthquake. Geophys. Res. Lett. 38, L09309. http://dx.doi.org/10.1029/2011GL047065.
Pritchard, M.E., Jay, J.A., Aron, F., Henderson, S.T., Lara, L.E., 2013. Subsidence at southern Andes volcanoes induced by the 2010 Maule, Chile earthquake. Nat. Geosci. 6, 632–636. http://dx.doi.org/10.1038/NGEO1855.
Ramos, V.A., Kay, S.M., 2006. Overview of the tectonic evolution of the southern Central Andes of Mendoza and Neuquén (35°–39°S latitude). In: En Kay, S.M., Ramos, V.A. (Eds.), Evolution of the Andean Margin: a Tectonic and Magmatic View from the Andes to the Neuquén Basin (35°–39°S Latitude), Geological Society of America, Special Paper 407, pp. 1–17.
Rietbrock, A., Ryder, I., Hayes, G., Haberland, C., Comte, D., Roecker, S., Lyon-Caen, H., 2012. Aftershock seismicity of the 2010 Maule Mw=8.8, Chile, earthquake: correlation between co-seismic slip models and aftershock distribution? Geophys. Res. Lett. 39, L08310. http://dx.doi.org/10.1029/2012GL051308.
Ryder, I., Rietbrock, A., Kelson, K., Burgmann, R., Floyd, M., Socquet, A., Vigny, C., Carrizo, D., 2012. Large extensional aftershocks in the continental forearc triggered by the 2010 Maule earthquake, Chile. Geophys. J. Int. 188, 879–890. http://dx.doi.org/10.1111/j.1365-246X.2011.05321.x.
Scott, Ch, Lohman, R., Pritchard, M., Alvarado, P., Sánchez, G., March 2014. Andean earthquakes triggered by the 2010 Maule, Chile (Mw 8.8) earthquake: comparisons of geodetic, seismic and geologic constraints. J. South Am. Earth Sci. 50, 27–39. http://dx.doi.org/10.1016/j.jsames.2013.12.001.
Sokos, E., y Zahradnik, J., 2008. ISOLA a Fortran code and a Matlab GUI to perform multiple-point source inversion of seismic data. Comput. Geosciences 34, 967–977.
Spagnotto, S.L., 2013. Sismicidad entre 34.5°-36.5°S y 67°-71°O posterior al sismo de Maule, Mw=8.8, 27/02/2010 y distribuciones de deslizamientos en placa de Nazca para sismos de profundidades mayores a 100 km en secciones plana y

normal entre 31–34°S" (Ph.D. thesis). Universidad Nacional de San Juan, Argentina.
Stein, R.S., 1999. The role of stress transfer in earthquake occurrence. Nature 402, 605–609.
Tapia, F., Farías, M., Naipauer, J., 2015. Late Cenozoic contractional evolution of the current arc-volcanic region along the southern Central Andes (35°20′S). J. Geodyn. 88, 36–51.
Taylor, M.A.J., Dmowska, R., Rice, J.R., 1998. Upper-plate stressing and seismicity in the subduction earthquake cycle. J. Geophys. Res. 103 (B10), 24523–24542 pp. L14317.
Toda, S., Stein, R.S., 2002. Response of the San Andreas fault to the 1983 Coalinga-Nuñez earthquakes: an application of interaction-based probabilities for Parkfield. J. Geophys. Res. 107 http://dx.doi.org/10.1029/2001JB000172.
Toda, S., Stein, R.S., Richards-Dinger, K., Bozkurt, S., 2005. Forecasting the evolution of seismicity in southern California: animations built on earthquake stress transfer. J. Geophys. Res. B05S16. http://dx.doi.org/10.1029/2004JB003415.
Tormey, D., 2010. Managing the effects of accelerated glacial melting on volcanic collapse and debris flows: Planchon–Peteroa Volcano, southern Andes. Glob. Planet. Change 74 (2), 82–90.
Tormey, D., Frey, F., y López-Escobar, L., 1989. Geologic history of the active Azufre-Planchón-Peteroa volcanic center (35°15′S, southern Andes) with implications for the development of compositional gaps. Rev. Assoc. Geol. Argent. 44 (1–4), 420–430.
Tormey, D., Frey, F., Lopez-Escobar, L., 1995. Geochemistry of the active Azufre–Planchon–Peteroa volcanic complex, Chile (35°15′S): evidence for multiple sources and processes in a cordilleran arc magmatic system. J. Petrol. 36, 265–298.
Vergani, G.D., Tankard, A.J., Belotti, H.J., y Welsink, H.J., 1995. Tectonic evolution and paleogeography of the Neuquén basin, Argentina. In: Tankard, A.J., Suárez, R.Y., Welsink, H.J. (Eds.), Petroleum Basins of South America, American Association of Petroleum Geologists, Memoir, vol. 62, pp. 383–402 (Tulsa).
Vigny, C., Socquet, A., Peyrat, S., Ruegg, J.C., Métois, M., Madariaga, R., Morvan, S., Lancieri, M., Lacassin, R., Campos, J., Carrizo, D., Bejar-Pizarro, M., Barrientos, S., Armijo, R., Aranda, C., Valderas-Bermejo, M.C., Ortega, I., Bondoux, F., Baize, S., Lyon-Caen, H., Pavez, A., Vilotte, J.P., Bevis, M., Brooks, B., Smalley, R., Parra, H., Baez, J.C., Blanco, M., Cimbaro, S., Kendrick, E., 2011. The 2010 Mw 8.8 Maule mega thrust earthquake of central Chile, monitored by GPS. Science 332 (6036), 1417–1421. http://dx.doi.org/10.1126/science.1204132.
Zahradnik, J., Serpetsidaki, A., Sokos, E., y Akis Tselentis, G., 2005. Iterative deconvolution of regional waveforms and a double-event interpretation of the 2003 Lefkada earthquake, Greece. Bull. Seismol. Soc. Am. 95 (1), 159–172. http://dx.doi.org/10.1785/0120040035.
Zoback, M.D., Zoback, M.L., 2002. Stress in the Earth's Lithosphere: Encyclopedia of Physical Science and Technology, Third ed., vol. 16. Academic Press, pp. 143–154.